J Mater Sci: Mater Electron
DOI 10.1007/s10854-015-4028-6

Growth of high quality $CH_3NH_3PbI_3$ thin films prepared by modified dual-source vapor evaporation

Ping Fan[1,2] · Di Gu[1] · Guang-xing Liang[1,2] · Ju-long Chen[1] · Jing-ting Luo[1,2] · Yi-zhu Xie[1] · Zhuang-hao Zheng[1,2] · Dong-ping Zhang[1,2]

Received: 9 August 2015 / Accepted: 2 November 2015

Abstract In this work, a high quality $CH_3NH_3PbI_3$ thin film prepared by modified dual-source vapor evaporation was proposed. An ultra-thin PbI_2 layer was deposited firstly, and then CH_3NH_3I and PbI_2 were evaporated simultaneously to form $CH_3NH_3PbI_3$ thin film. The results show that flat, uniform, smooth, less porous and good crystallinity perovskite thin films without impure phase are formed by the modified dual-source vapor evaporation. The ratios of Pb/I accord with the nominal $MAPbI_3$ stoichiometry and the band gaps are about 1.60 eV close to the theoretical value of 1.55 eV. The properties of $CH_3NH_3PbI_3$ thin film fabricated by this method are suitable for perovskite solar cells applications.

1 Introduction

Solar is an emerging excellent energy due to the properties of clean, renewable and reliable. In the recent years, organic–inorganic hybrid perovskite solar cell has become the hottest topic in the photovoltaic area [1–5]. What is more, the power conversion efficiency (PCE) of perovskite solar cells has skyrocketed to 20.3 % [2] since it reported in 2009 by Miyasaka group [1] in the first time. The great achievement of perovskite solar cells mostly benefits from their unique structures, excellent properties of electrical, magnetic, and optical [4–6]. To date, various processing approaches, such as one step solution method [7–9] and two step sequential solution deposition [10–12], vacuum deposition [13–17] and vapor-assisted solution processing [18], have been reported to fabricate the perovskite layer in order to get a expected absorbed layer with the properties of good morphology, desired crystallization and accurate stoichiometry ratio. Among all methods, dual-source vapor evaporation has the best control on the morphology and crystallization, due to the forming process in the vapor environment with the best control and least contamination [14]. In this progress, methyl-ammonium iodide (CH_3NH_3I) and lead chloride ($PbCl_2$) with an excess molar ratio about 4:1 were put in separate sources firstly, and then the CH_3NH_3I and $PbCl_2$ were evaporated simultaneously from the vacuum cavity bottom when the pressure was below 10^{-5} mbar [14]. The annealing procedure is necessary to form a fully crystallization perovskite layer at last. And the vapour deposited perovskite device got an efficiency of 15.4 % [14]. However, it is hard to control the evaporation rates and the reaction between the different vapor molecules of the $PbCl_2$ and MAI sources simultaneously, specially, the CH_3NH_3I molecular weight is really small, which is hard to monitoring deposition rate. As a variation to the dual-source vapor evaporation, Lin reported a simple layer-by-layer sequential vacuum deposition which deposited a prepared $PbCl_2$ layer firstly, and then a CH_3NH_3I layer was deposited upon the $PbCl_2$ layer sequentially, in this way, the $PbCl_2$ layer was converted to perovskite in situ by reacting with the CH_3NH_3I [17]. This progress is simpler and has better control on the CH_3NH_3I than the conventional vapor evaporation. However, it also meets the difficulty that it is really hard for CH_3NH_3I

✉ Ping Fan
fanping308@126.com

✉ Guang-xing Liang
lgx@szu.edu.cn

[1] Institute of Thin Film Physics and Applications, College of Physics Science and Technology, Shenzhen University, Shenzhen 518060, China

[2] Shenzhen Key Laboratory of Sensor Technology, Shenzhen University, Shenzhen 518060, China

Published online: 11 November 2015

molecules to access and fully react with inner PbI_2 layer as similar as the problem of two step sequential solution deposition [12, 18].

In this paper, we introduced a modified progress of $CH_3NH_3PbI_3$ thin film fabrication via modified dual-source vapor evaporation. As show in Fig. 1, the PbI_2 powder was heated separately to form an ultra-thin PbI_2 layer, and then the CH_3NH_3I and PbI_2 were evaporated simultaneously. As we can see that the sequential progress is as same as the conventional dual-source vapor evaporation, but it is different from both the dual-source vapor evaporation and simple layer-by-layer sequential vacuum deposition. In this method, it can balance the stoichiometry ratio by the ultra-thin PbI_2 layer and avoids the difficulty of CH_3NH_3I molecules to access and fully react with inner PbI_2 layer. Therefore, the expected $CH_3NH_3PbI_3$ thin film with the properties of good morphology, desired crystallization and accurate stoichiometry ratio was prepared by the modified dual-source vapor evaporation.

2 Methods

2.1 Thin film preparation

2.1.1 CH_3NH_3I synthesis

CH_3NH_3I was fabricated by reacting 28 ml of CH_3NH_2 (40 wt% in water, Xiya Reagent) and 30 ml of HI (57 wt% in water, Xiya Reagent) in a round bottom flask which had been kept at 0 °C for 2 h with constant magnetic stirring. Sequentially the white CH_3NH_3I crystals were made by evaporating the solution at 60 °C for 2 h. Then diethyl ether was used to purify the CH_3NH_3I crystals. At last, in order to dry the CH_3NH_3I crystals, they were stayed at 60 °C in vacuum oven for 24 h [5–7].

2.1.2 $CH_3NH_3PbI_3$ thin films via modified dual-source vapor evaporation

Firstly, 110 mg of PbI_2 powder was placed into a crucible and 160 mg of CH_3NH_3I was placed into another crucible. Secondly, the source of PbI_2 was heated slowly by increasing the evaporating power when the pressure in the chamber was about 1×10^{-3} pa, and then the power of PbI_2 source was kept 400 W for 5 min to deposit an ultra-thin PbI_2 layer. Thirdly, the power of the source of CH_3NH_3I was increased slowly to 200 W. In this procedure, the CH_3NH_3I and PbI_2 were evaporated simultaneously for 20 min. At last, the as-prepared samples were annealed at 100 for 30 min in the vacuum chamber.

2.2 Characterization

1. XRD. X-Ray diffraction (XRD) technique (Ultima IV) was used to measure the crystallographic structure of films. And the instrument operated at 40 kV and 40 mA with CuKα radiation (0.15406 nm).
2. EDS. An energy dispersive X-ray microanalysis system (Model: BRUKER QUANTAX 200) attached to SEM was used for obtaining the composition and element mapping of $CH_3NH_3PbI_3$ thin films via modified dual-source vapor evaporation.
3. SEM. Surface and cross-sectional images of $CH_3NH_3PbI_3$ thin films were analyzed by a SUPRA 55 scanning electron microscopy (SEM) which used an electron beam accelerated at 5 kV.
4. Optical transmittance. Optical transmittance properties of the perovskite films were obtained by ultraviolet (UV)/visible (VIS)/near-infrared (NIR) spectrophotometer (Lambda 950, Perkin Elemer).
5. Film thickness. The prepared film thickness was measured by DEKTAK XT profilometer.

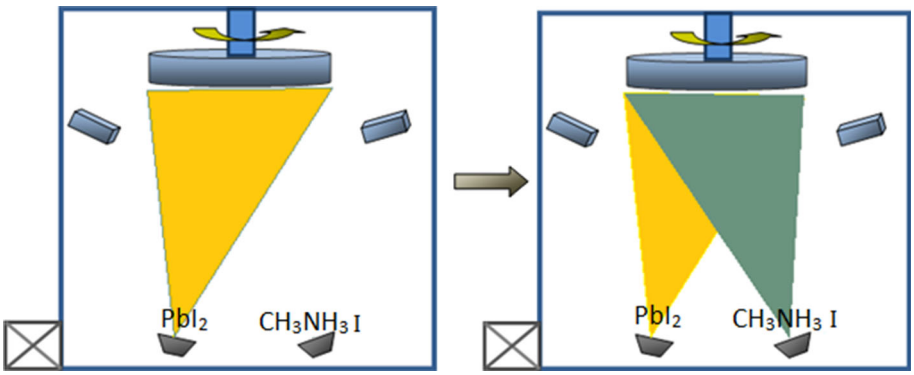

Fig. 1 Modified dual-source thermal evaporation system for depositing the $CH_3NH_3PbI_3$ thin films

3 Results and analysis

In order to study the formation of perovskite phases and crystallization, XRDwas measured. As shown in Fig. 2, both as-prepared and annealed thin films have a set of preferred orientation XRD peaks at 14.04, 28.28, 31.76, 40.52 and 43.06, which are assigned to (110), (220), (310), (224) and (330) plane, respectively, and confirm that the $CH_3NH_3PbI_3$ perovskite is tetragonal structure [18–20]. Surprising, the preferred orientation XRD peaks is sharp, clearly indicating a good crystallinity of perovskite prepared by this method. What is more, there are none peaks from the impurity phase, especially the MAI and PbI_2 phase, in the XRD patterns, indicating that the formation of perovskite phases via modified dual-source vapor evaporation is pure.

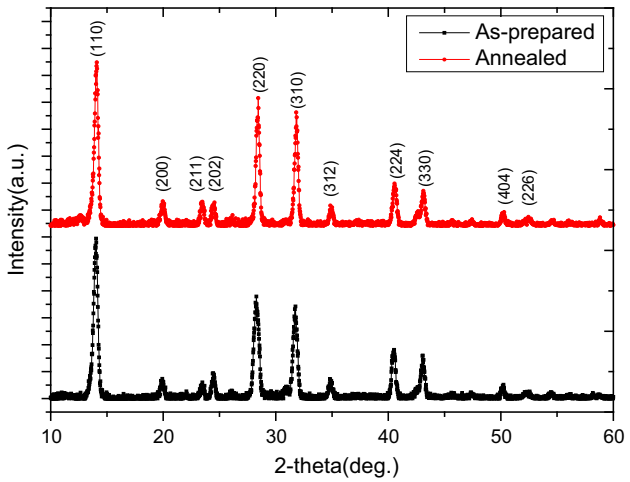

Fig. 2 XRD patterns of $CH_3NH_3PbI_3$ thin films via modified dual-source vapor evaporation

In order to review the degree of preferential orientation in the films, the TC_{hkl} [texture coefficient of the (hkl) plane] is defined as the degree of as the percent of intensity of plane (hkl) to the sum of intensities of all planes in the X-ray pattern [21].

$$TC_{hkl} = I_{hkl} \Big/ \sum\nolimits_{all} I_{hkl} \quad (1)$$

where I_{hkl} is the intensity of the (hkl) plane. As shown in Fig. 3a, there are three gradient value of TC_{hkl} in both as-prepared and annealed thin films, the maximum gradient is TC110 which is about 35 %, the medial gradient are TC_{220} and TC_{310} about 25 %, and the minimum gradient are TC_{224} and TC_{330} about 9 %. There is an obvious chance in TC_{hkl} between the as-prepared and annealed film, after annealing, the values of the maximum gradient and the minimum gradient decrease, yield the value of the medial gradient increases, indicating that preferential orientation of (220) and (310) planes enhance. What is more, the full width at half maximum (FWHM) and the crystallite size are shown in Fig. 3b. The FWHM values of (110) and (224) are almost equal. Yet the FWHM values of (110) and (224) are induce from 0.442 to 0.317 and from 0.37 to 0.299, respectively. In contrast, the value of (330) increases from 0.382 to 0.482. Due to the Scherrer's equation, the chances of the crystallite size are consistent with the chances in FWHM pattern. All of them indicate that the crystallite size of (220) and (310) planes enhance, which is consistent with the analyses from texture coefficient.

The composition of $MAPbI_3$ thin films is an important factor, which influences the properties of structural, electrical and optical of absorbers. As shown in Fig. 4, the compositional analyses are measured by EDS technique, there are two feature peaks at 2.48 and 3.98 keV which are assigned to Pb and I element, respectively. Due to the as-prepared thin film compositional analyses, as shown in

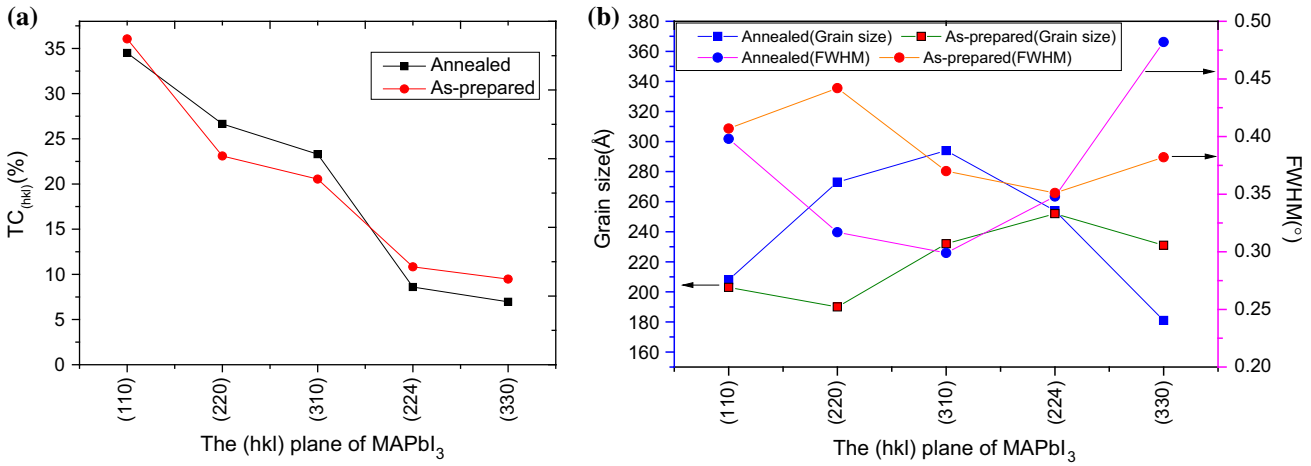

Fig. 3 Variation of **a** texture coefficients for selected diffracting planes, **b** crystallite size and FWHM

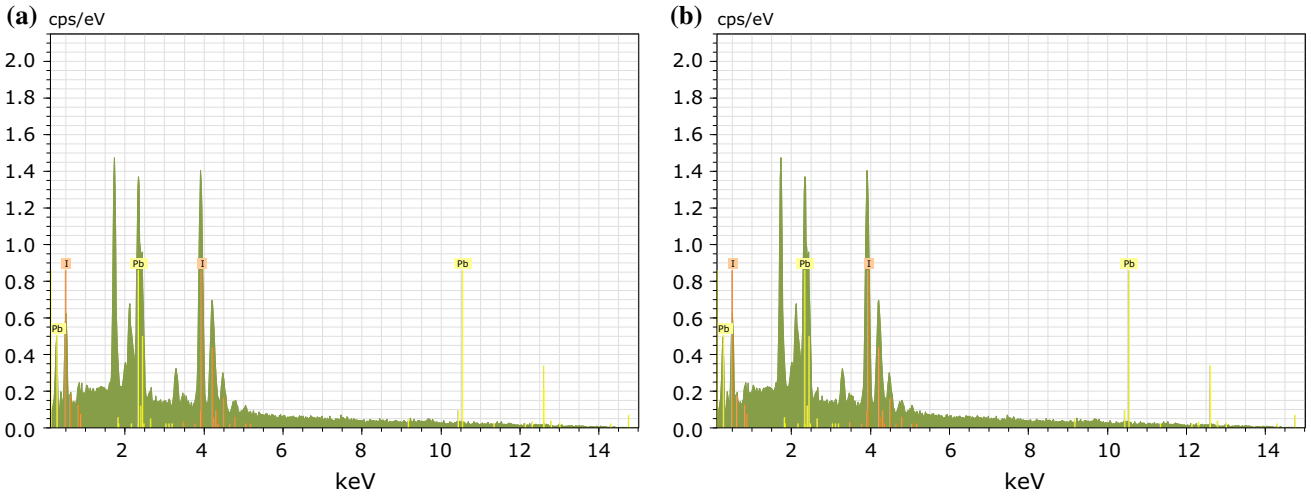

Fig. 4 EDS spectral line pattern of $CH_3NH_3PbI_3$ thin films via modified dual-source vapor evaporation (**a** As-prapeared perovskite film, **b** anealed perovskite film)

Table 1 Elemental composition of $CH_3NH_3PbI_3$ thin films via modified dual-source vapor evaporation

The modified dual-source vapor evaporation	At.%		Pb/I
	Pb	I	
As-prepared thin film	24.02	75.98	0.316
Annealed thin film	24.41	75.59	0.323

Table 1, it is found that the percent of atomicity of Pb and I are 24.02 and 75.98 %, respectively. In contrast, the value of Pb element increases to 24.41 % consistent with the value of I element 75.59 % after the annealed progress, indicating that the CH_3NH_3I reacted with PbI_2 fully via the modified dual-source vapor evaporation. Amazingly, the ratio of Pb/I, expressly in the annealed thin film, are close to the nominal $MAPbI_3$ thin films stoichiometry about 0.33

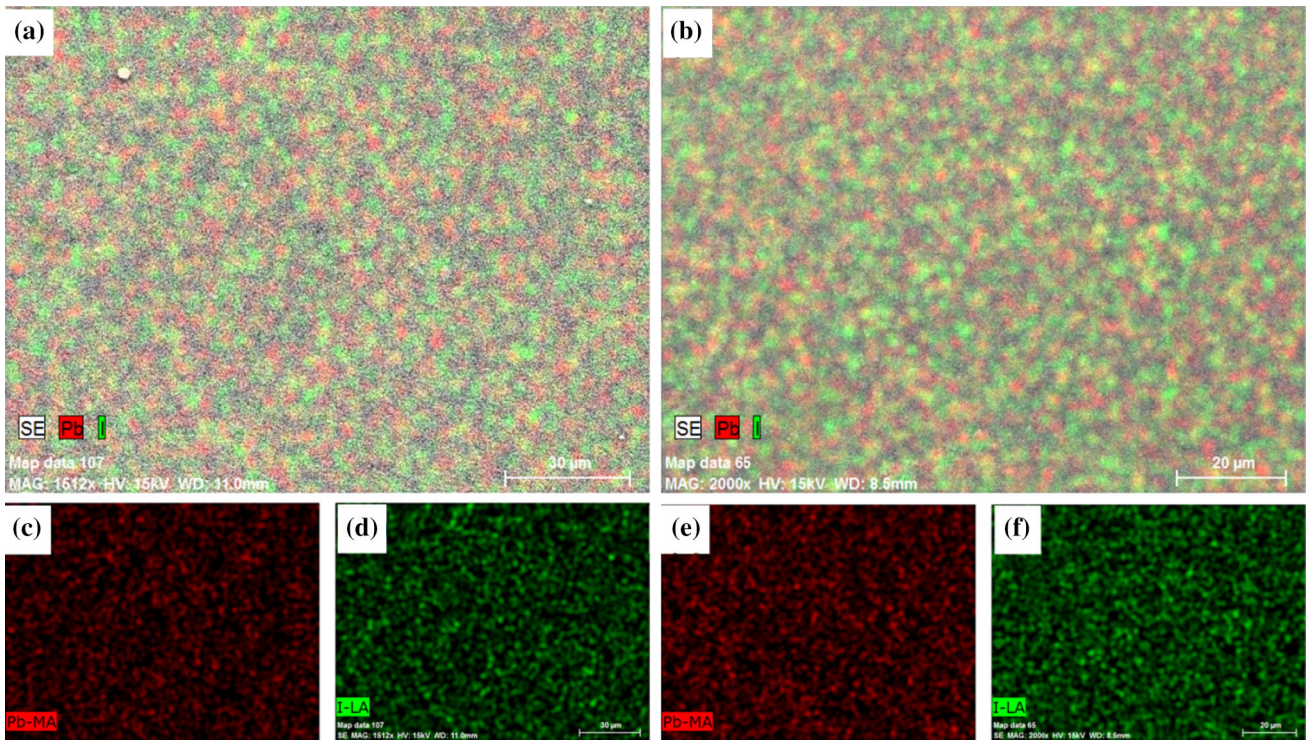

Fig. 5 EDS-MAP of the $CH_3NH_3PbI_3$ thin films via modified dual-source vapor evaporation (**a**, **c**, **d** As-prapeared perovskite film, **b**, **e**, **f** anealed perovskite film)

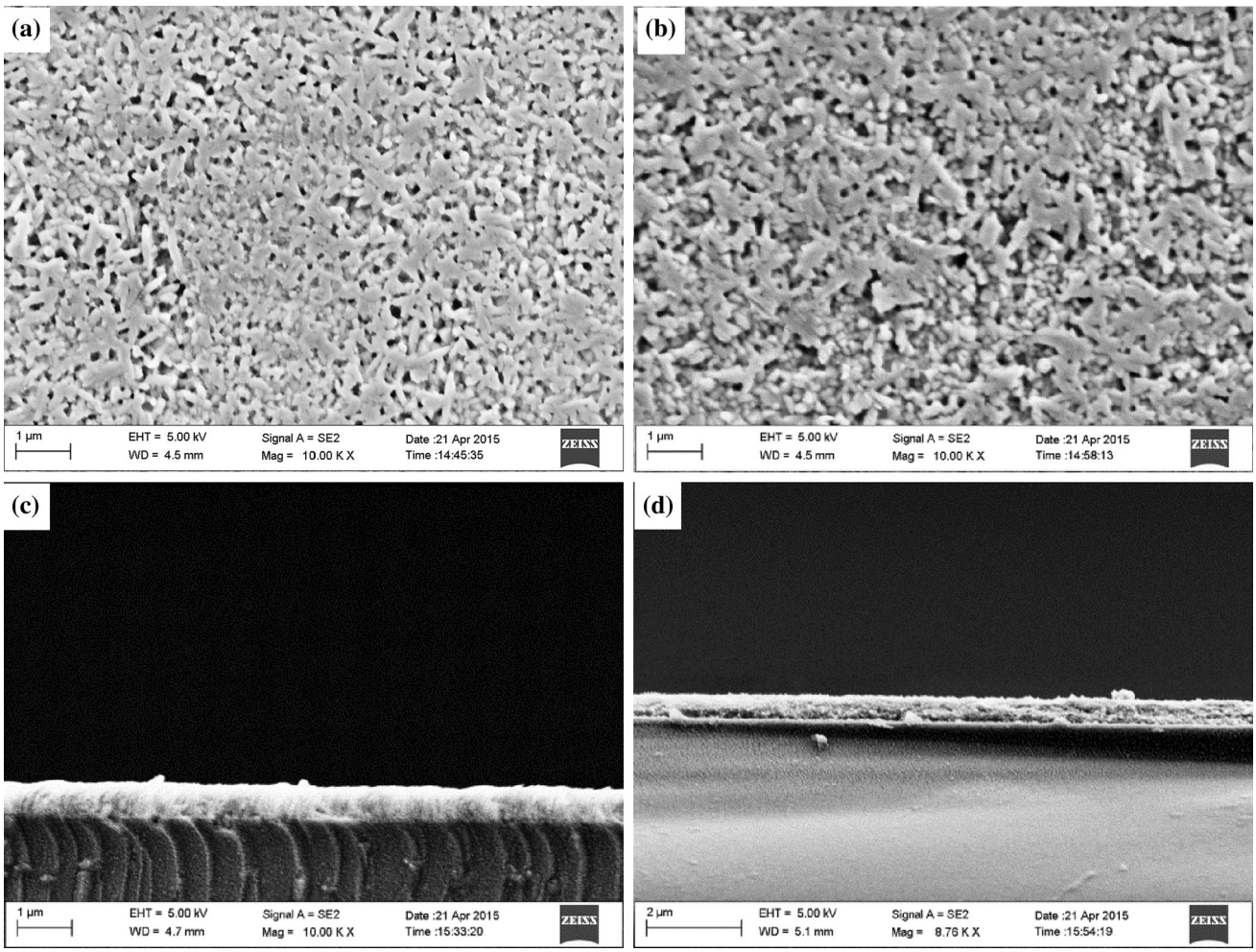

Fig. 6 Surface and cross-sectional SEM images of $CH_3NH_3PbI_3$ thin films via modified dual-source vapor evaporation (**a**, **c** As-prapeared perovskite film, **b**, **d** anealed perovskite film)

[19], which confirms that the modified dual-source vapor evaporation can balance the stoichiometry ratio by the ultra-thin PbI_2 layer and avoids the difficulty of CH_3NH_3I molecules to access and fully react with inner PbI_2 layer. What is more, as shown in Fig. 5, the position of Pb and I element are nearly homogeneous in the entire plane, which takes advantage from the modified dual-source evaporation technology.

The morphology of $CH_3NH_3PbI_3$ thin film was measured by the SEM images, as shown in Fig. 6a, there are obvious particles, which are homogeneous and uniform grain size, in the thin film, clearly indicating a good crystallinity of perovskite prepared by the modified dual-source vapor evaporation. What is more, after annealed progress, the grain sizes increase notably in Fig. 6b, indicating that the crystallinity in annealed thin film is better than that in as-prepared thin film, which is consistent with the analyses from XRD before. As show in Fig. 6c, d, the cross-sectional of $CH_3NH_3PbI_3$ thin films, which thickness is approximately 700 nm, are really flat, uniform, compact, non-pinholes. What is more, there is only a total layer which indicates that CH_3NH_3I molecules are reacting with PbI_2 fully without excrescent element left. All properties of morphology confirm that $CH_3NH_3PbI_3$ thin film via the modified dual-source evaporation technology would be an appropriate absorbed layer [22].

In order to study the optical character of $CH_3NH_3PbI_3$ thin films, the transmittance analysis was measured by spectrophotometer. As shown in Fig. 7, the transmittance of $CH_3NH_3PbI_3$ thin films with heat-treating is similar to the as-prepared film. The transmittances of them were low nearly to 0 % in the visible region, however, almost 80 % in the wavelength span from 800 to 2000 nm. Amazingly, there was a sharp absorption edge on set of 800 nm [23, 24], which indicated that $CH_3NH_3PbI_3$ thin films had the advantage of the large light absorption over the whole visible solar emission spectrum due to the good crystallinity and expected morphology of thin films prepared by

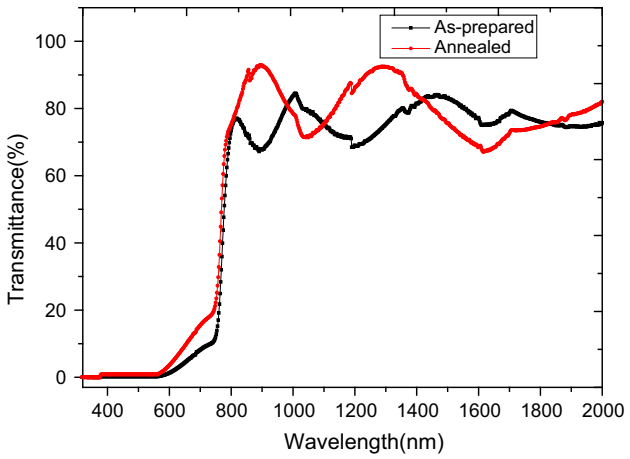

Fig. 7 The transmittance analysis results of $CH_3NH_3PbI_3$ thin films via modified dual-source vapor evaporation

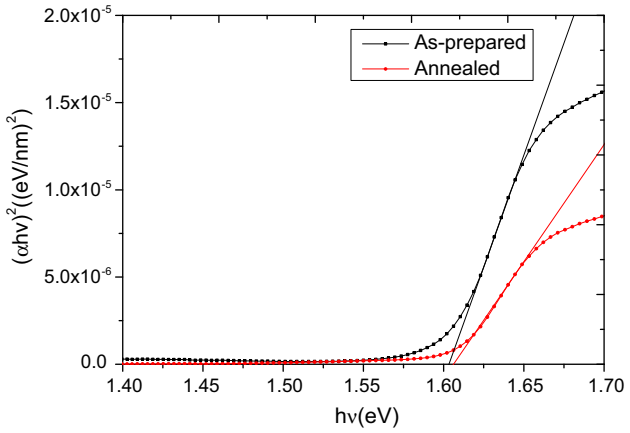

Fig. 8 The optical band gap estimation for $CH_3NH_3PbI_3$ thin films via modified dual-source vapor evaporation

the modified dual-source evaporation technology. What is more, the band gap energy was calculated from

$$(\alpha hv)^2 = A(hv - E_g) \quad (2)$$

where α is absorption coefficient, hv is photon energy, A is a constant, E_g is the band gap energy [25]. As shown in Fig. 8, the results revealed that the band gaps of as-prepared and annealed thin film are about 1.60, 1.61 eV, respectively. Both of them are closely to the theoretical value of 1.55 eV reported by Baikie [23].

4 Conclusion

In summary, we reported a modified progress of $CH_3NH_3PbI_3$ thin film fabrication via modified dual-source vapor evaporation. The PbI_2 powder was heated separately to form an ultra-thin PbI_2 layer, and then the CH_3NH_3I and PbI_2 were evaporated simultaneously. It balanced the stoichiometry ratio by the ultra-thin PbI_2 layer and avoids the difficulty of CH_3NH_3I molecules to access and fully react with inner PbI_2 layer. The microstructure, composition, morphology and optical properties of $CH_3NH_3PbI_3$ thin films were characterized with XRD, EDS, SEM and spectrophotometer technique, respectively. The results show that the $CH_3NH_3PbI_3$ perovskite is tetragonal structure with a good crystallinity without impure phase. The ratios of Pb/I are close to the nominal $MAPbI_3$ stoichiometry about 0.33. What is more, the $CH_3NH_3PbI_3$ thin films are really flat, uniform, compact, less porous. At last, the band gaps of thin film are about 1.60 eV close to the theoretical value of 1.55 eV. All properties of $CH_3NH_3PbI_3$ thin film via this method indicating its promising applicability for high performance of Perovskite solar cells.

Acknowledgments This work was supported by National Natural Science Foundation of China (Grant No. 61404086), Basical Research Program of Shenzhen (JCYJ20150324140036866), the special fund of the central finance for the development of local Universities (Grant No. 000022070150), the innovation development fund project of graduate student 2015 (Grant No. 0003600206).

References

1. A. Kojima, K. Teshima, Y. Shirai et al., Organometal halide perovskites as visible-light sensitizers for photovoltaic cells. J. Am. Chem. Soc. **131**, 6050–6051 (2009)
2. N.J. Jeon, J.H. Noh, W.S. Yang et al., Compositional engineering of perovskite materials for high-performance solar cells. Nature **517**, 476–480 (2015)
3. Q. Wang, H. Chen, G. Liu et al., Control of organic–inorganic halide perovskites in solid-state solar cells: a perspective. Sci. Bull. **60**, 405–418 (2015)
4. D.B. Mitzi, Templating and structural engineering in organic–inorganic perovskites. J. Chem. Soc., Dalton Trans. **1**, 1–12 (2001)
5. D. Shi, V. Adinolfi, R. Comin et al., Solar cells. Low trap-state density and long carrier diffusion in organolead trihalide perovskite single crystals. Science **347**, 519–522 (2015)
6. Z. Xiao, Y. Yuan, Y. Shao et al., Giant switchable photovoltaic effect in organometal trihalide perovskite devices. Nat. Mater. **14**, 193–198 (2015)
7. M. Xiao, F. Huang, W. Huang et al., A fast deposition-crystallization procedure for highly efficient lead iodide perovskite thin-film solar cells. Angew. Chem. **53**, 9898–9903 (2014)
8. H. Zhou, Q. Chen, G. Li et al., Interface engineering of highly efficient perovskite solar cells. Science **345**, 542–546 (2014)
9. J.H. Heo, S.H. Im, J.H. Noh et al., Efficient inorganic–organic hybrid heterojunction solar cells containing perovskite compound and polymeric hole conductors. Nat. Photonics **7**, 486–491 (2013)
10. J. Burschka, N. Pellet, S.J. Moon et al., Sequential deposition as a route to high-performance perovskite-sensitized solar cells. Nature **499**, 316–319 (2013)
11. G.E. Eperon, V.M. Burlakov, P. Docampo et al., Morphological control for high performance, solution-processed planar heterojunction perovskite solar cells. Adv. Funct. Mater. **24**, 151–157 (2014)

12. A. Dualeh, N. Tétreault, T. Moehl et al., Effect of annealing temperature on film morphology of organic–inorganic hybrid pervoskite solid-state solar cells. Adv. Funct. Mater. **24**, 3250–3258 (2014)
13. Q. Lin, A. Armin, R.C.R. Nagiri et al., Electro-optics of perovskite solar cells. Nat. Photonics **9**, 106–112 (2014)
14. M. Liu, M.B. Johnston, H.J. Snaith, Efficient planar heterojunction perovskite solar cells by vapour deposition. Nature **501**, 395–398 (2013)
15. L.K. Ono, S. Wang, Y. Kato et al., Fabrication of semi-transparent perovskite films with centimeter-scale superior uniformity by the hybrid deposition method. Energy Environ. Sci. **7**, 3989–3993 (2014)
16. G.-X. Liang, P. Fan, J.-T. Luo et al., A promising unisource thermal evaporation forin situfabrication of organolead halide perovskite $CH_3NH_3PbI_3$ thin film. Prog. Photovoltaics Res. Appl. **22**, 1 (2015). doi:10.1002/pip.2632
17. A. Ng, Z.W. Ren, Q. Shen et al., Efficiency enhancement by defect engineering in perovskite photovoltaic cells prepared using evaporated PbI_2/CH_3NH_3I multilayers. J. Mater. Chem. A **3**, 9223–9231 (2015)
18. Q. Chen, H. Zhou, Z. Hong et al., Planar heterojunction perovskite solar cells via vapor-assisted solution process. J. Am. Chem. Soc. **136**, 622–625 (2014)
19. Y. Zhao, K. Zhu, CH3NH3Cl-assisted one-step solution growth of $CH_3NH_3PbI_3$: structure, charge-carrier dynamics, and photovoltaic properties of perovskite solar cells. J. Phys. Chem. C **118**, 9412–9418 (2014)
20. H.B. Kim, H. Choi, J. Jeong et al., Mixed solvents for the optimization of morphology in solution-processed, inverted-type perovskite/fullerene hybrid solar cells. Nanoscale **6**, 6679–6683 (2014)
21. J. He, L. Sun, Y. Chen et al., Influence of sulfurization pressure on Cu_2ZnSnS_4 thin films and solar cells prepared by sulfurization of metallic precursors. JPS **273**, 600–607 (2015)
22. F. Huang, Y. Dkhissi, W. Huang et al., Gas-assisted preparation of lead iodide perovskite films consisting of a monolayer of single crystalline grains for high efficiency planar solar cells. Nano Energy **10**, 10–18 (2014)
23. T. Baikie, Y. Fang, J.M. Kadro et al., Synthesis and crystal chemistry of the hybrid perovskite $(CH_3NH_3)PbI_3$ for solid-state sensitised solar cell applications. J. Mater. Chem. A **1**, 5628 (2013)
24. J. Shi, Y. Luo, H. Wei et al., Modified two-step deposition method for high-efficiency $TiO_2/CH_3NH_3PbI_3$ heterojunction solar cells. ACS Appl. Mater. Interfaces **6**, 9711–9718 (2014)
25. J. Müller, J. Nowoczin, H. Schmitt, Composition, structure and optical properties of sputtered thin films of $CuInSe_2$. Thin Solid Films **496**, 364–370 (2006)